This article is licensed under CC-BY 4.0 CC



pubs.acs.org/IC

Article

# Gold(I) Complexes with Bulky Phosphanes: A Dual Approach to **Triplet Harvesting and Hydroamination Catalysis**

Araceli de Aquino, Nazaret Santamaría, Artur J. Moro, David Aguilà, Auxiliadora Prieto, M. Carmen Nicasio,\* João Carlos Lima,\* and Laura Rodríguez\*



Cite This: Inorg. Chem. 2025, 64, 3392-3402



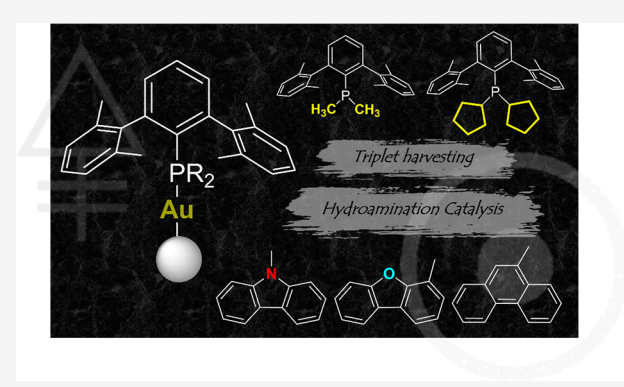
**ACCESS** I

III Metrics & More

Article Recommendations

Supporting Information

ABSTRACT: Two families of mononuclear gold(I) complexes featuring Au-chromophore units, with chromophores being carbazole (a), phenanthrene (b), or dibenzofuran (c), were synthesized. The Au(I) atoms are coordinated to two phosphanes, either PMe<sub>2</sub>Ar<sup>Xyl2</sup>  $(Ar^{Xyl2} = 2,6-C_6H_3-(2,6-C_6H_3-Me_2)_2)$  (P1) or the bulkier  $PCyp_2Ar^{Xyl2}$  (Cyp = cyclopentyl) (P2). The photophysical properties of these complexes were extensively studied, with a particular focus on the effects of phosphane bulkiness and chromophore electrondonating capacity on triplet state quantum yields  $(\Phi_T)$ . Nanosecondlaser flash photolysis measurements were employed to calculate  $\Phi_T$ . Time-dependent density functional theory (TD-DFT) calculations supported the absorption and emission assignments, providing insights into the electronic state gaps involved in photophysical



processes and their relative populations. The parent complex AuClP2 in combination with NaBAr<sub>4</sub><sup>F</sup>, as a chloride scavenger, served as an efficient catalyst for the hydroamination of a variety of alkynes and amines, under mild conditions and with low Au loading (0.1-0.2 mol %). Luminescent studies allowed us to check the active catalytic species.

# INTRODUCTION

Phosphorescence emission is strongly sought due to its wide range of applications such as in photodynamic therapy, oxygen sensing,<sup>2</sup> light-emitting diodes (PhOLEDs),<sup>3,4</sup> or photon upconversion, 5,6 among others. To achieve this kind of emission, it is mandatory to control and understand the formation of T<sub>n</sub> states, which are responsible for the phosphorescence in the first step, and later the ratio between the rates for radiative and nonradiative decay of the triplets returning to the ground state.

When the phosphorescent emitters are incorporated in electrically excited devices (e.g. light emitting devices, LEDs), the triplet states can significantly increase the internal quantum efficiency of the device emission due to the spin-statistics, since 75% of the excitons are known to populate triplet states, compared with the 25% that produce  $S_n$  states.

To populate the triplet state photophysically, we need to enhance the intersystem crossing transition  $(S_1 \rightarrow T_n)$ , since only the  $S_0 \rightarrow S_1$  is allowed upon optical excitation. The intersystem crossing transition is favored by the presence of heavy metal atoms, that increase the spin-orbit coupling and facilitate the transfer of the S<sub>1</sub> excitons obtained by optical excitation to  $T_n$  states. Specifically, we use gold(I) for this purpose, as it is known to exhibit the highest spin-orbit coupling among the d-block metals.  $^{8-11}$ 

Gold(I) compounds can also display the so-called metallophilic interactions,  $^{12-14}$  which can affect their photophysical properties. 15,16 In our group, we have recently investigated the influence of aurophillic contacts (Au···Au) and its nature (either intra- or intermolecular) in the harvesting of the  $T_n$ states.17

In this work, we aim to explore new methods for modulating the population of  $T_n$ . To achieve this, we prepared two families of compounds with the structure chromophore-Au-PR3 and their AuClPx precursors (Px = P1 and P2). The chromophores used are carbazole (Cz), dibenzofuran (Fu), and phenanthrene (Phen), selected for their varying electrondonating abilities to study their effects on the promotion of  $T_n$ . The luminescent ligands carbazole, phenanthrene, and dibenzofuran were chosen for their distinct electronic properties to systematically study their impact on photophysical behavior. Carbazole, as a strong electron donor, enhances conjugation and triplet state formation but lowers fluorescence quantum yields due to efficient intersystem crossing (ISC).

Received: November 20, 2024 Revised: December 30, 2024 Accepted: January 30, 2025 Published: February 11, 2025





Phenanthrene, with moderate electron-donating ability, balances fluorescence and phosphorescence, offering insight into  $S_1$ - $T_1$  transitions. Dibenzofuran, the weakest electron donor, shows the highest fluorescence yields by favoring radiative decay pathways and minimizing ISC.

Additionally, we used two different phosphanes with varying steric volumes,  $PMe_2Ar^{xyl2}$  (P1) and  $PCyp_2Ar^{xyl2}$  (P2), to examine how the ligand bulkiness influences intermolecular interactions and, consequently, the population of  $T_n$ . In our previous work, we demonstrated that the conformation of phosphanes could promote either intramolecular or intermolecular aurophilic contacts due to the specific arrangement of the molecules. In the current study, we will investigate the influence of the phosphane bulk on the  $T_n$  harvesting process to determine if this factor is crucial for optimizing the triplet state population.

Moreover, electron-rich ancillary ligands with high steric demand have proven to be superior in gold(I)-catalyzed hydroamination reactions. <sup>18,19</sup> In particular, ligands with a pendant group that stabilizes the gold center through secondary interactions enhance substantially the catalytic activity of the Au(I) complexes. Thus, highly competent gold(I) catalysts with phosphane<sup>20</sup> or NHC<sup>21</sup> ancillary ligands have been designed, which enable the hydroamination of primary amines and alkynes at catalyst loadings lower than 0.5 mol % under mild reaction conditions. Terphenyl phosphanes can stabilize low-coordinate structures by adopting hemilabile coordination modes involving weak M···C<sub>arene</sub> interactions with a flanking aryl ring of the terphenyl moiety.<sup>22</sup> Herein, we demonstrate the excellent catalytic performance of our gold(I) compounds in the intermolecular alkyne hydroamination.<sup>23,</sup> Furthermore, emission experiments allowed us to verify the stability of the catalyst during the reaction. This additional exploration aims to expand the potential applications of these gold(I) compounds beyond their photophysical properties.

# ■ RESULTS AND DISCUSSION

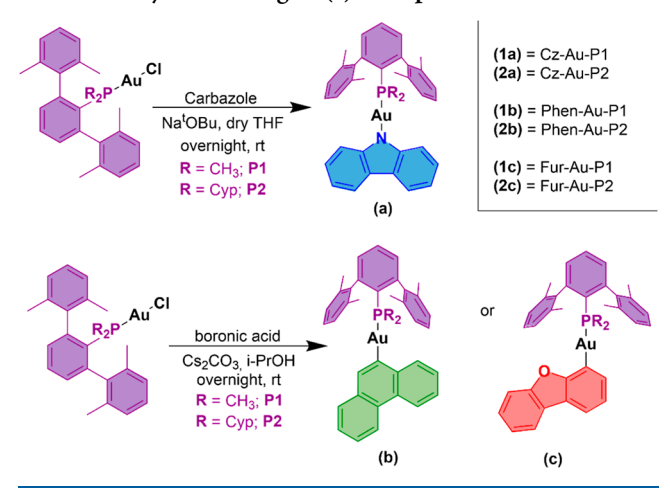
**Synthesis and Characterization.** Two families of mononuclear gold(I) compounds with phosphanes displaying different levels of bulkiness have been synthesized following a two-step synthesis. Initially, the phosphane—Au—Cl derivatives were prepared by the reaction of AuCl(tht) and the corresponding phosphane (Scheme S1).

In the second step, AuClP1 and AuClP2 were reacted with three chromophores that present different electron-donating or electron-withdrawing properties (carbazole (a), phenanthrene (b), dibenzofuran (c)) following two different reaction conditions displayed in Scheme 1.

For the synthesis of 1a and 2a, the precursor AuClPx was dissolved together with the carbazole ligand La in the presence of NaO<sup>t</sup>Bu and the reaction mixture was allowed to react overnight at room temperature in dry THF. However, the coordination of either phenanthrene (b) or dibenzofuran (c) to the metal center was achieved following our previously reported procedure. A solution of the corresponding boronic acid derivative with the AuClPx compound was reacted in the presence of  $Cs_2CO_3$  in 2-propanol at room temperature overnight (see Experimental Section for details). All the compounds were characterized by  $^1H$ ,  $^{13}C\{^1H\}$ , and  $^{31}P\{^1H\}$  NMR spectroscopy and mass spectroscopy (see Supporting Information).

Single crystals suitable for X-ray diffraction analysis were successfully grown for 1a, 1b, 2b, and 2c (Figure 1) from slow

Scheme 1. Synthesis of gold(I) Complexes 1a-c and 2a-c



diffusion of hexane into dichloromethane solutions of the compounds at room temperature. The crystal data and structure refinement can be found in Table S1, and the selected bond distances and angles are displayed in Table 1.

The coordination of the gold(I) unit to the corresponding atom from the fluorophore is almost linear with slightly distorted C-Au-P or N-Au-P angles from 168° to 176°, with compound 2b being the most distorted one and the carbazole derivative 1a the most linear. The corresponding packing of the molecules is, as expected, being affected by the bulkiness of the phosphanes.  $\pi \cdots \pi$  and  $C-H\cdots \pi$  weak intermolecular contacts between the carbazole groups and aromatic rings of the phosphane can be detected in compounds 1a and 1b (Figures S38 and S39). Meanwhile, the X-ray crystal structures of the compounds containing the bulkier phosphane (P2) shows dimeric assemblies in a headto-tail conformation, where two molecules interact through  $C-H\cdots\pi$  contacts as can be seen in Figure 2. No metallophilic intermolecular interactions were detected for none of the compounds independently of the bulkiness of the phosphane.

Photophysical Characterization. The absorption and emission spectra of all the compounds 1(a-c) and 2(a-c)were recorded in dichloromethane solutions at room temperature. The obtained data are summarized in Table 2. The electronic absorption spectra of all the complexes show an intense band at ca. 310 nm for La and Lb ligands and at ca. 290 nm for Lc. These bands are red-shifted upon coordination to the metal center (Figure 3). These transitions can be assigned to ligand-centered  $\pi - \pi^*$  transitions according to the literature. 26-28 The higher energy absorption band around 260 nm is ascribed to the Px moieties (see Figure S40). All compounds display a well-resolved emission band at 377 nm for a and b derivatives and at 340-350 nm for c derivatives ascribed to ligand-to-ligand charge transfer fluorescence transitions (see below theoretical calculations) 17,28-30 (Figure 3). The emission lifetimes in the order of nanoseconds and the small Stokes' shifts agree with this fluorescence emission assignment.

As shown in Table 2, compounds with dibenzofuran as the chromophore, 1c, 2c, exhibit the highest fluorescence quantum yield values  $(\Phi_{FI})$ , whereas carbazole derivatives have the lowest values at room temperature. The recorded fluorescence quantum yields, and decay times are not significantly affected by the presence of oxygen in the samples (Figures S41, S42, S46–S57).

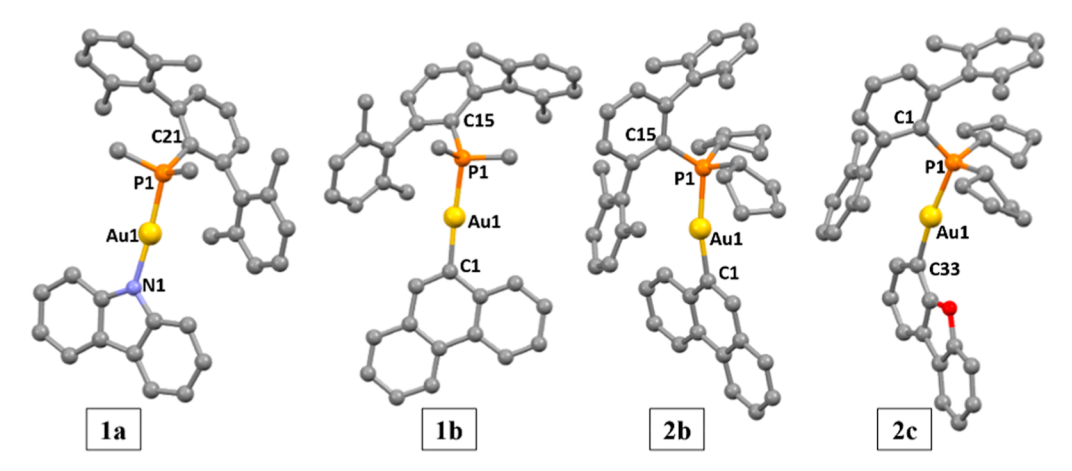
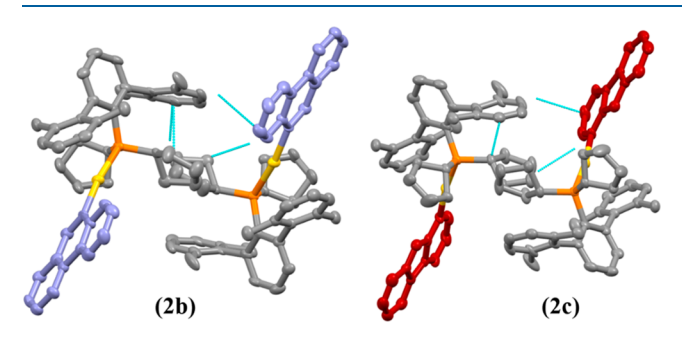


Figure 1. X-ray crystal structures of gold(I) compounds 1a, 1b, 2b, and 2c. Yellow: gold; orange: phosphorus, blue: nitrogen, red: oxygen; gray: carbon. Thermal ellipsoids at 50% probability and hydrogen atoms were omitted for clarity.

Table 1. Selected Bond Lengths (Å) and Angles (°) for Complexes 1a, 1b, 2b, and 2c

1a		1b		2b		2c	
			Distan	ces (Å)			
N1-Au1	2.044(2)	C1-Au1	2.070(4)	C1-Au1	2.06(1)	C33-Au1	2.054(7)
Au1-P1	2.248(8)	Au1-P1	2.301(9)	Au1-P1	2.306(2)	Au1-P1	2.299(2)
	Angles (°)						
N1-Au1-P1	175.99(7)	C1-Au1-P1	173.5(1)	C1-Au1-P1	168.7(3)	C33-Au1-P1	171.7(2)
Au1-P1-C21	114.06(9)	Au1-P1-C15	118.3(1)	Au1-P1-C15	122.4(3)	Au1-P1-C1	120.6(2)



**Figure 2.** 3D crystal packing and intermolecular interactions present at complexes **2b** and **2c** viewed down the *b*-axis. Yellow: gold; orange: phosphorus, blue: nitrogen, gray: carbon. Thermal ellipsoids at 50% probability and hydrogen atoms were omitted for clarity. The chromophores have been colored in order to clearly see the head-totail conformation. Dashed lines represent the  $C-H\cdots\pi$  contacts.

Phosphorescence emission at room temperature can be detected at ca. 480 nm only for phenanthrene derivatives (1b

and **2b**) after removing O<sub>2</sub> from the solutions (Figure 4), while the other gold(I) complexes do not present any variation under these experimental conditions (Figures S41 and S42).

At low temperatures, the emission of all gold(I) complexes is dominated by the phosphorescence band (see Figure S43), indicating that despite the absence of phosphorescence at room temperature, all complexes have a substantial increase in the triplet state population when compared to the organic precursors L(a-c). This is due to enhanced intersystem crossing from the lowest singlet excited state to the triplet manifold which is also responsible for the significant decrease in the observed fluorescence quantum yields of the complexes relative to L(a-c). Absorption and emission spectra were also recorded for the Px and AuClPx precursors (see Figure S44). The Px ligands exhibit emission bands at 353 and 365 nm for P1 and P2, respectively. These emissions are significantly quenched upon coordination to the Au(I) center in the AuClPx compounds. As expected, intersystem crossing (ISC) processes are much more efficient in the AuClPx compounds.

Table 2. Absorption and Emission Maxima and Fluorescence Quantum Yield Data of the gold(I) Derivatives in Dichloromethane at Room Temperature

compound	absorption $\lambda_{\max}$ (nm), (10 <sup>4</sup> $\varepsilon$ (M <sup>-1</sup> cm <sup>-1</sup> ))	fluorescence emission, $\lambda_{\rm exc}$ = 311 (a,b), 280 (c) nm; (solution, $\lambda_{\rm max}$ (nm))	fluorescence quantum yield $(\Phi_{Fl})$	fluorescence quantum yield $N_2$ sat. $\left(\Phi_{Fl}\right)$
La	292 (1.67)	355	$0.22 (\pm 0.02)$	0.25 (±0.02)
1a	306 (1.26)	382	$0.02 \ (\pm 0.002)$	$0.04 \ (\pm 0.003)$
2a	308 (1.05)	380	$0.03 \ (\pm 0.002)$	0.09 (±0.007)
Lb	299 (0.92)	372	$0.04 (\pm 0.003)$	$0.06 \ (\pm 0.005)$
1b	310 (1.42)	380	$0.07 (\pm 0.006)$	0.07 (±0.006)
2b	311 (1.21)	376	$0.07 (\pm 0.006)$	$0.07 \ (\pm 0.006)$
Lc	289 (1.37)	330	$0.35 (\pm 0.03)$	$0.34 (\pm 0.03)$
1c	288 (1.64)	345	$0.12 (\pm 0.009)$	$0.13 (\pm 0.01)$
2c	288 (1.61)	345	$0.14 (\pm 0.01)$	$0.15 \ (\pm 0.01)$

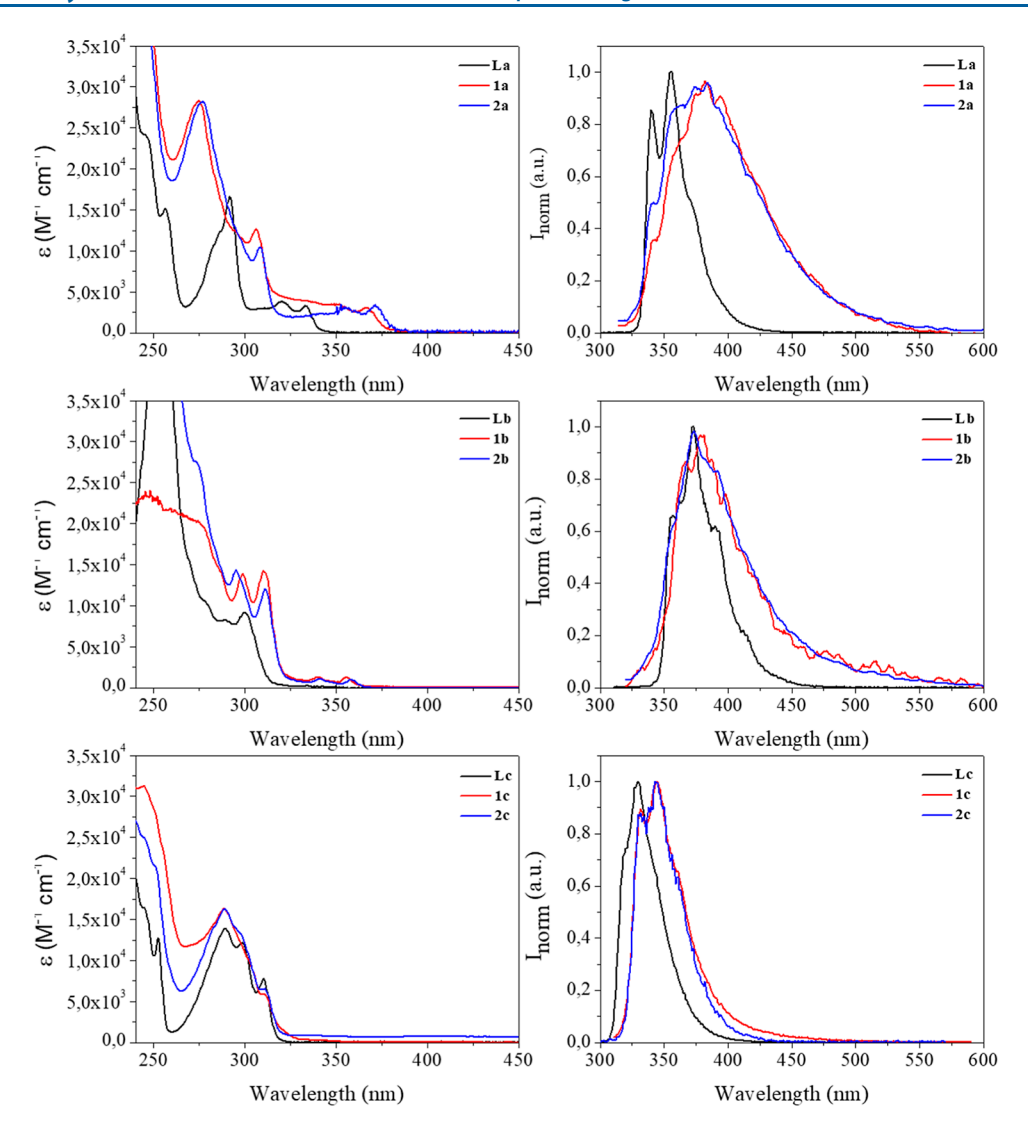


Figure 3. Absorption (left) and emission,  $\lambda_{\text{exc}} = 310$  nm (a and b derivatives), and 290 nm (c derivatives) (right) spectra of dichloromethane solutions of complexes 1(a-c) and 2(a-c) at room temperature.

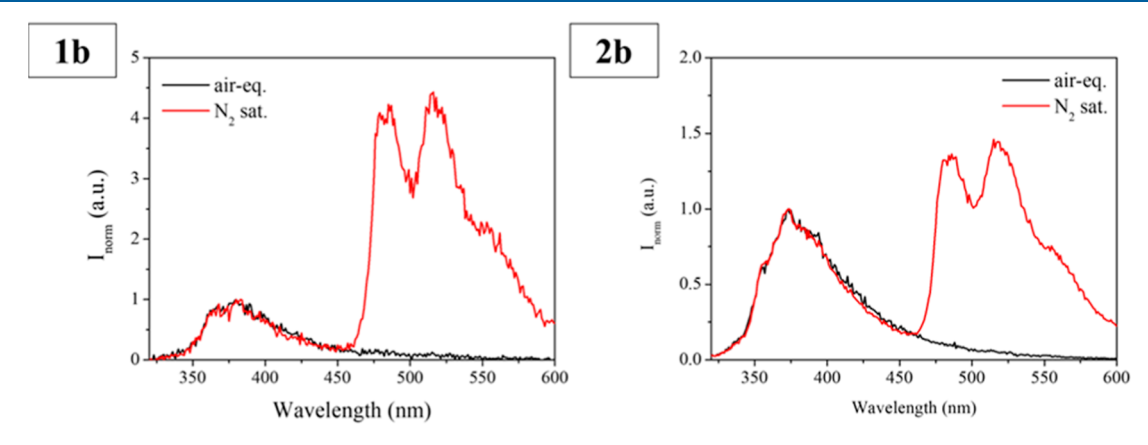


Figure 4. Emission spectra of  $N_2$  saturated dichloromethane solutions of complexes 1b (left) and 2b (right) at room temperature.  $\lambda_{exc} = 311$  nm.

This is evidenced by the spectra recorded at 77 K, where the gold(I) complexes show pure phosphorescence, in contrast to the dual emission observed for the uncoordinated Px ligands.

**Triplet Formation Quantum Yield.** Quantum yields of triplet formation,  $\Phi_T$ , and triplet decay times in the presence and absence of oxygen were measured using nanosecond

transient absorption, and the results are summarized in Table 4. The steric properties of both phosphanes have been calculated with the percent buried volume (% $V_{\rm bur}$ ) parameter and the topographic steric maps using the SambVca~2.1 web application  $^{31-33}$  (Figure S45) for comparison purposes since we aimed to determine whether its bulkiness could affect the

photophysical parameters with impact in the triplet state population. The rate constants related to the intersystem crossing ( $k_{\rm ISC}$ ) and the  $S_0 \leftarrow S_1$  internal conversion transition ( $k_{\rm IC}$ ) have been calculated (see Supporting Information, eqs 4 and 5). The steric maps are viewed down the z-axis, and the orientation of ligands is also indicated in the figure. The red and blue zones show the more- and less-hindered parts in the ligand, respectively. As can be seen, **P2** is significantly bulkier in comparison to **P1**, with a % $V_{\rm bur}$  of 42.9 and 34.2%, respectively. As expected, the areas more hindered are those where the substituents CH<sub>3</sub> or Cyp are localized.

The transient decay times recorded for the gold(I) complexes (Figures S57–S68) are in the range of nanoseconds when oxygen is present in the solution and increase to the microseconds range (Table 4 and Supporting Information) in the absence of oxygen, confirming efficient quenching of the triplet state by molecular oxygen, being potential candidates for producing singlet oxygen (see below).

From the decay times in Table 3 and the triplet quantum yields in Table 4, it is possible to calculate the values for the

Table 3. Fluorescence Decay Times Values of Aerated Solutions and  $N_2$ -Saturated Solutions in DCM Recorded for all the Compounds

Compound	au (air-equilibrated) (ns)	$\tau$ (N <sub>2</sub> ) (ns)
1a	6.2 (±0.3)	5.9 (±0.3)
2a	$7.6 \ (\pm 0.4)$	$9.3 (\pm 0.5)$
1b	11.4 (±0.6)	14.0 $(\pm 0.7)$
2b	$12.9 \ (\pm 0.6)$	$16.7 \ (\pm 0.8)$
1c	2.3 (±0.1)	$3.0 \ (\pm 0.1)$
2c	$3.2 (\pm 0.2)$	3.6 (±0.2)

Table 4. Quantum Yields of Triplet Population for the Dichloromethane Solutions  $(\Phi_{\rm T})$ , Decay Times in Air-Equilibrated,  $\tau_{\rm T}({\rm O_2})$ , and Nitrogen Saturated,  $\tau_{\rm T}({\rm N_2})$ , Dichloromethane Solutions; Rate Constants for Intersystem Crossing  $(k_{\rm ISC})$  and Singlet Internal Conversion to the Ground State  $(k_{\rm IC})$ 

compound	$\Phi_{\mathrm{T}}$	$ au_{\mathrm{T}}\left(\mathrm{O}_{2} ight) \\ \left(\mathrm{ns}\right)$	$ au_{\mathrm{T}} \left( \mathrm{N}_{2} \right) \ \left( \mu \mathrm{s} \right)^{b}$	$k_{\rm ISC} \ (10^6 \ {\rm s}^{-1})$	$k_{\rm IC} \ (10^6 \ {\rm s}^{-1})$
1a	18.9	30	8.7	32.0	131.2
2a	44.3	50	5.5	47.6	50.7
1b	29.0°	323	15.5	20.7	46.1
2b	43.0 <sup>a</sup>	187	5.5	25.8	30.2
1c	47.1	150	1.5	157.0	133.0
2c	37.2	183	0.4	103.3	134.2

"Quantum yield of triplet formation estimated from the quantum yield of singlet oxygen production (see below). "These values are in microseconds while those in air-equilibrated conditions are in nanoseconds."

intersystem crossing rate constant,  $k_{\rm ISC}$ , as well as the values for the rate constant of internal conversion between  $S_1$  and  $S_0$ . There is a clear correlation between  $k_{\rm ISC}$ , and  $k_{\rm IC}$  in the large majority of the cases, but 1a represents a notable exception with a very large internal conversion rate constant. This could suggest that there is a similar contribution from molecular vibrations to facilitate both singlet relaxation pathways: the internal conversion for the ground state and the intersystem crossing to the triplet state, also observed for metal-free organic molecules. <sup>34</sup>

We anticipate that the rate constant for intersystem crossing  $(k_{\rm IC})$  is influenced by the bulk and rigidity of the phosphanes, but we could also expect an impact in  $k_{\rm ISC}$ , since it was shown that intermolecular gold—gold interactions can affect the intersystem crossing. While the first phenomenon occurs because steric hindrance likely restricts some vibrations within the medium, resulting in a diminished contribution to the vibrational relaxation process, the latter is related to the steric hindrance for the formation of intermolecular gold···gold contacts.

In the case of **a** and **b** it is clear that the bulkier the phosphane, the smaller the corresponding  $k_{\rm IC}$ , with a small impact in  $k_{\rm ISC}$ , while in the case of **c**, the largest phosphane has an impact in a decrease of  $k_{\rm ISC}$ , which could be evidence for some degree of intermolecular association affecting the retrieved constants.

Singlet Oxygen Production. The efficient quenching of the triplet state of the gold(I) complexes by molecular oxygen is generally related to energy transfer leading to  $^1\text{O}_2$  photosensitization or the presence of other mechanisms involving oxygen, e.g. electron transfer. The direct measurement of the characteristic  $^1\text{O}_2$  emission at 1270 nm, which belongs to  $^1\Delta_g \to {}^3\Sigma_g^-$  transition, was used as a direct proof of this photosensitization process.

To do that, the samples were excited at  $\lambda_{\rm exc}=311$  nm in airequilibrated dichloromethane solutions and using perinaphthenone as the reference ( $\Phi_{\Delta}=79\%$ ). Dibenzofuran complexes (1c and 2c) have technical difficulties that make not possible the measurement of the  $^1{\rm O}_2$  production.

The triplet formation quantum yields of the phenanthrene gold(I) complexes were not accessible through ns-laser flash photolysis measurements using the depletion method (strong overlap between ground state bleaching and triplet absorption) but were able to display a significant production of  $^1\mathrm{O}_2$  under our experimental conditions, with  $\Phi_\Delta$  values of 29% for 1b and 43% for 2b (Figure S69).

The measured  $\Phi_\Delta$  values are always in the lower limit of the  $\Phi_T$  of the photosensitizer, i.e., assuming an efficiency of energy transfer to oxygen close to unity yields  $\Phi_\Delta=\Phi_T$ , and lower efficiencies lead to higher values of  $\Phi_T^{~36}$ 

Theoretical Calculations. TD-DFT calculations were conducted for all compounds to optimize geometries without restraints, and harmonic frequency calculations confirmed converged structures as potential-energy minima. These calculations were performed with continuum solvation in dichloromethane, primarily to identify the lower singlet and triplet states of the molecules. All compounds present monoexcitations involving the highest occupied molecular orbital (HOMO) and the lowest unoccupied molecular orbital (LUMO). Figures \$70-\$75 show these molecular orbitals for all of them, and Tables \$3-\$5 summarize the obtained results.

It is anticipated that the most significant intersystem crossing transitions will occur between the  $S_1$  state and the energetically closest  $T_n$  state with suitable symmetry<sup>37</sup> (see Tables S3–S5, where the most probable  $T_n$  state is highlighted in bold). The corresponding values from TD-DFT calculations are also presented in Table 5.

Interestingly, compounds with larger values of  $\Delta E(S_1-T_1)$  also exhibit higher fluorescence quantum yields  $(\Phi_{FI})$ . This observation aligns with less efficient intersystem crossing in compounds with a larger energy gap, thereby increasing the probability of  $S_1$  returning to  $S_0$  through an emissive decay.

Table 5. Calculated Energy Differences between  $S_1-T_1$  and  $S_1-T_n^{\ a}$ 

compound	$\Delta E(S_1 - T_1)$ (meV)	$\Delta E(S_1 - T_n)$ (meV)	$k_{\rm ISC}~(10^6~{\rm s}^{-1})$
1a	173.5	23.8	32.0
2a	165	24.6	47.6
1b	1102.6	171.1	20.7
2b	1089.8	192.4	25.8
1c	1121.2	3.1	157.0
2c	1112.7	6.1	103.3

<sup>a</sup>The values of  $k_{\rm ISC}$  have been extracted from Table 4 for clarity.

There is a clear correlation observed in Table 5 between the smaller singlet—triplet energy gap  $(\Delta E(S_1-T_n))$  and the more efficient ISC process. That is,  $k_{\rm ISC}$  dibenzofuran (c) > carbazole (a) > phenanthrene (b), while the  $\Delta E(S_1-T_n)$ , for dibenzofuran (c) < carbazole (a) < phenanthrene (b). However, due to the complex interplay of vibrational modes and internal conversion, this correlation does not straightforwardly translate into an increase in  $\Phi_{\rm T}$  across all cases. Conversely, the  $S_1-T_1$  energy gap shows a weak correlation with  $k_{\rm ISC}$  suggesting that intersystem crossing likely occurs between  $S_1$  and higher triplet states.

Catalytic Studies. The dual utility of chloride gold(I) complexes (AuClP1 and AuClP2) is a cornerstone of this study, bridging photophysical applications and catalytic functionality. The chloride complexes serve not only as precursors for the luminescent compounds but also demonstrate exceptional activity in hydroamination catalysis. This dual functionality underscores the versatility of the complexes and highlights the critical role of the bulky phosphane ligands. To assess the impact of the steric profile of terphenyl phosphanes on gold-catalyzed alkyne hydroamination, we screened the catalytic competency of the gold AuClPx compounds<sup>38</sup> in the hydroamination of phenylacetylene with aniline (Table 6).

The reactions were performed in the presence of equimolar amounts of the gold complex and the chloride scavenger NaBAr<sub>4</sub><sup>F</sup> (Ar<sup>F</sup> = 3,5-(CF<sub>3</sub>)<sub>2</sub>C<sub>6</sub>H<sub>3</sub>), using reaction conditions similar to those reported for other ligands for ease of comparison. We found that both AuClPx complexes were active in the hydroamination of a 1:1 neat mixture of the alkyne and the amine with 0.1 mol % of the gold catalyst and NaBAr<sub>4</sub><sup>F</sup> at 50 °C (Table 6, entries 1 and 2). However,

(NHC)AuCl/NaBAr4F

8

only complex AuClP2 supported by the bulkier terphenyl phosphane, PCyp<sub>2</sub>Ar<sup>Xyl2</sup> provided complete conversions. Consequently, further catalytic tests were conducted only with AuClP2. We observed excellent conversions when the hydroamination was performed at room temperature with 0.1 mol % AuClP2/NaBAr<sub>4</sub><sup>F</sup> (entry 3). A further reduction of the catalyst loading to 0.05 mol % still provided the imine in a high 86% yield, albeit to reach full conversion the mixture required heating at 50 °C (entries 4 and 5). The catalytic activity displayed by AuClP2/NaBAr<sub>4</sub><sup>F</sup> under such mild reaction conditions compares well to those observed for the most efficient Au(I) catalysts under similar conditions (entries 6–8).

We examined the scope of the hydroamination reactions with different alkynes and a variety of aryl amines under the optimized reaction conditions (Scheme 2). Both, electron-rich and electron-deficient anilines added to phenylacetylene at room temperature affording the corresponding imines in good to high yields (Scheme 2, ab-ad). Sterically hindered anilines such as mesitylamine and 2,6-diisopropylphenylamine were also suitable substrates for the addition of phenyl acetylene at 50 °C (ae and af). Regarding the alkyne scope, p-substituted phenylacetylenes with different electronic demands, as well as alkylacetylenes underwent hydroamination with aniline, although reactions of the latter required increasing the catalyst loading to 0.2 mol % (ag-aj). Diphenylacetylene, a reluctant substrate that usually requires high catalyst loadings and harsher reaction conditions to accomplish this transformation,<sup>39</sup> could be successfully functionalized using 0.2 mol % catalyst at 80 °C, providing the expected hydroamination product in good yield as a 3:1 mixture of the imine and enamine derivatives (ak). Finally, we sought to test the reactivity of the gold catalysts in the amination of phenylacetylene with challenging secondary amines. 396,c The corresponding enamines were obtained in good yields with 2.5 mol % of gold catalyst (al, am). With N-methylaniline the reaction yielded exclusively the Markonikov adduct, whereas with piperidine a mixture 1:3 of the Markonikov and anti-Markonikov products was obtained. Overall, these results demonstrate the excellent performance of the terphenyl phosphane ligand PCyp<sub>2</sub>Ar<sup>Xyl2</sup> in gold-catalyzed hydroamination of alkynes.

The catalytic reaction was followed by emission spectroscopy in order to monitor the catalyst stability over time (see Figure S76). As stated above, the demetalation of the catalyst

76

Table 6. Catalytic Activity of AuCl(PR<sub>2</sub>Ar<sup>Xyl2</sup>) in the Hydroamination of Phenylacetylene with Aniline<sup>a</sup>

	Ph─ <b>=</b> +	PhNH <sub>2</sub> (PR <sub>2</sub> Ar <sup>Xyl2</sup> )Au	ıCl/NaBAr <sup>F</sup> 4	N <sup>Pn</sup>	
	FII — +	neat,	24 h	Ph	
entry	catalyst	Au (mol %)	T (°C)	conversion (%)	TON
1	AuClP1	0.1	50	59	590
2	AuClP2	0.1	50	98	980
3	AuClP2	0.1	25	99 (96) <sup>b</sup>	960
4	AuClP2	0.05	25	86	1720
5	AuClP2	0.05	50	99 (94) <sup>b</sup>	1980
6	Y <sub>Mes</sub> PCy <sub>2</sub> AuCl/NaBAr <sub>4</sub> <sup>F</sup>	0.05	50	97	1950 <sup>c</sup>
7	$(CB_{11}Cl_{11})PiPr_2Au(THT)$	0.01	50	>95	>9500 <sup>d</sup>

<sup>&</sup>lt;sup>a</sup>Reaction conditions: phenylacetylene (5 mmol), aniline (5 mmol), Au(I) complex: NaBAr<sub>4</sub><sup>F</sup> = 1:1, reaction time = 24 h (unoptimized). Conversions determined by GC using dodecane as an internal standard. <sup>b</sup>Yields of isolated products are given in brackets. <sup>c</sup>From ref 20c. <sup>d</sup>From ref 20a (reaction time 16 h). <sup>e</sup>From ref 21 (Au(I) complex: NaBAr<sub>4</sub><sup>F</sup> = 1:16; reaction time = 37 h).

80

0.01

7600°

Scheme 2. Intermolecular Hydroamination of Alkynes with Primary and Secondary Aryl Amines Catalysed by  $AuClP2/NaBAr_4^F$ 

"Reaction conditions: phenylacetylene (2.5 mmol), aniline (2.5 mmol). Yields of isolated product.  ${}^bT = 50 \, {}^\circ\text{C}$ . Catalyst loading (0.2 mol %).  ${}^dT = 80 \, {}^\circ\text{C}$ . Selectivity imine/enamine 3:1 determined by  ${}^1\text{H}$  NMR. Selectivity loading (2.5 mol %). Selectivity gem/E/Z = 1:1.4:1.4 determined by  ${}^1\text{H}$  NMR.

should induce an increase on the emission intensity of the phosphane, what would indicate the degradation of the catalyst along the reaction process. The reason for this emission enhancement is that the loss of gold(I) leads to a decrease on the quenching mechanism imposed by the intersystem crossing. As we did not observe any increase in the emission intensity, this means that the phosphane is kept coordinated to the metal center without degradation. Additionally, if phosphane decoordination occurs, it should be accompanied by the reduction of Au(I) to Au(0), which is readily observable to the naked eye. The persistence of the yellow color throughout the reaction, along with its intensification during the formation of the final product, further supports the stability of the AuClPx catalyst.

By modulating steric hindrance through these ligands, we observed significant effects on both photophysical parameters, such as quantum yield  $(\Phi_{\rm T})$  and intersystem crossing rates  $(k_{\rm ISC})$ , and catalytic efficiency. For instance, **P2**, with its bulkier cyclopentyl substituents, enhances the stabilization of intermediates in hydroamination reactions, leading to superior catalytic performance even under mild conditions. Simultaneously, the steric bulk influences the suppression of nonradiative decay pathways in photophysical processes,

allowing higher triplet state populations. Thus, the interconnection lies in the shared dependency of both applications on ligand steric and electronic properties. Increasing steric bulk provides a dual advantage by optimizing both photophysical performance and catalytic functionality.

## CONCLUSIONS

This work highlights the dual role of bulky gold(I) complexes as both efficient phosphorescent materials and robust hydro-amination catalysts. The X-ray structures obtained for compounds 1a, 1b, 2b, and 2c revealed the significant role of the presence of two different monophosphanes with varying bulkiness in the 3D packing of gold(I) derivatives. The bulk of these monophosphanes was found to influence molecular vibrations in the medium, resulting in differences in the  $k_{\rm IC}$  rate constants, typically higher for the smaller phosphane.

Three chromophores with distinct electron-donating capabilities were utilized: carbazole (a), phenanthrene (b), and dibenzofuran (c). All gold(I) compounds exhibited fluorescence emission at room temperature, while only phenanthrene derivatives showed phosphorescence under nitrogen-saturated conditions. However, all gold(I) compounds demonstrated phosphorescence when cooled to 77 K.

 $\Phi_{\rm T}$  was measured for all complexes, with  $\Phi_{\Delta}$  taken rigorously as  $\Phi_{\rm T}$  for phenanthrene derivatives. Rate constants  $k_{\rm IC}$  and  $k_{\rm ISC}$  were calculated, with compounds featuring dibenzofuran as the chromophore displaying the highest  $k_{\rm ISC}$  values.

The stabilization of the gold(I) center through steric bulk ensures excellent activity and selectivity in hydroamination reactions, with potential implications for broader catalytic applications. By elucidating these connections, this study not only advances the understanding of gold(I) complexes but also provides a framework for their application in interdisciplinary research.

All in all, it can be said that (i) The bulky phosphane ligands enhance triplet harvesting by modulating intersystem crossing rates and suppressing nonradiative decay pathways; (ii) the stabilization of the gold(I) center through steric bulk ensures excellent activity and selectivity in hydroamination reactions, with potential implications for broader catalytic applications; (iii) the interplay of steric and electronic effects in ligand design offers a pathway to multifunctional complexes for advanced material and catalytic applications.

By elucidating these connections, this study not only advances the understanding of gold(I) complexes but also provides a framework for their application in interdisciplinary research.

#### EXPERIMENTAL SECTION

**General Procedures.** All manipulations have been performed under prepurified  $N_2$  using standard Schlenk techniques. All solvents have been distilled from appropriate drying agents. Commercial reagents dibenzofuran-4-boronic acid and 9-phenanthreneboronic acid were purchased from Fluorochem, while cesium carbonate carbazole and NaOʻBu were purchased from Merck. Phosphanes  $PMe_2Ar^{Xyl2}$ ,  $^{40}$  P1 and  $PCyp_2Ar^{Xyl2}$ ,  $^{22a}$  P2 were prepared by previously reported procedures.

**Crystal Data.** Data for compounds **1a**, **1b**, **2b**, and **2c** were collected at BL13-XALOC beamline <sup>41</sup> of the ALBA synchrotron ( $\lambda$  = 0.72931) at 100 K. Crystals were mounted with Paratone N grease on a MiTegen kapton loop and placed in the N<sub>2</sub> stream of an Oxford Cryosystems Cryostream. The structures were solved by intrinsic phasing with SHELXT<sup>42</sup> and refined by full-matrix least-squares on  $F^2$  with SHELXL. <sup>43</sup>

**Physical Measurements.** Infrared spectra have been recorded on a Fourier transform infrared (FT-IR) 520 Nicolet Spectrophotometer.  $^1\mathrm{H}$  NMR ( $\delta(\mathrm{TMS})=0.0$  ppm) and  $^{31}\mathrm{P}\{^1\mathrm{H}\}$  NMR ( $\delta(85\%~\mathrm{H}_3\mathrm{PO}_4)=0.0$  ppm) spectra have been obtained on a Bruker 400. ES(+) mass spectra were recorded on a Fisons VG Quatro spectrometer. Absorption spectra have been recorded on a Varian Cary 100 Bio UV spectrophotometer, and emission spectra have been recorded on a Horiba Jobin-Yvon SPEX Nanolog spectrofluorimeter. Quantum yields have been recorded on a Hamamatsu Absolute PL Quantum Yield Spectrometer C11347. Luminescence lifetimes were measured on JYF-DELTAPRO-NL equipment upon excitation of the samples with a 285 nm NanoLED and collecting the decays through a bandpass filter of 340, 400, or 500 nm.

Transient absorption experiments were measured with a laser flash photolysis LK60 Applied Photophysics system in absorption mode after laser pulse excitation at 355 nm (for 1a, 2a and 1b, 2b) and 266 nm (for 1c, 2c) at the Departamento de Quimica-Universidade Nova de Lisboa.

**Theoretical Calculations.** Density functional calculations were carried out by using the GAUSSIAN package. <sup>44</sup> The geometries of all compounds in this study were fully optimized at the TZVP level of theory using Gaussian09. The hybrid density function method known as B3LYP was applied. <sup>45,46</sup> Effective core potentials (ECP) were used to represent the innermost electrons of the gold atom and the basis set of valence triple- $\zeta$  quality with an extra d-polarization function. <sup>47</sup>

A similar description was used for all main group elements.<sup>48</sup> Atomic charges and population analysis have been confirmed from the analysis of natural bond order.<sup>49</sup> The solvent effects of dichloromethane were taken into account by PCM calculations,<sup>50</sup> keeping the optimized geometries for the gas phase without symmetry restrictions. Excited states and absorption spectra were obtained from the time-dependent algorithm implemented in Gaussian09.<sup>51</sup>

Synthesis and Characterization. Synthesis of [AuCl-(PMe<sub>2</sub>Ar<sup>Xyl2</sup>)], AuClP1. AuCl(tht) (236.1 mg, 0.74 mmol) and P1 (PMe<sub>2</sub>Ar<sup>Xyl2</sup>) (255.1 mg, 0.74 mmol) were solved in a dichloromethane solution under Schlenk conditions and stirred at room temperature for 1 h. Then, the solution was concentrated, and hexane was added in order to precipitate the compound in a pure form. In the end, the solution is filtrated, and the white solid obtained is completely dried under vacuum. Yield 90% (383.9 mg). <sup>1</sup>H NMR (400 MHz, CDCl<sub>3</sub>, 25 °C,  $\delta$ ): 7.60 (td, 1H,  ${}^{3}J_{HH} = 7.5$  Hz,  ${}^{5}J_{HP} = 2$ Hz, p-C<sub>6</sub>H<sub>3</sub>), 7.29 (t, 2H,  ${}^{3}J_{HH} = 7.6$  Hz, p-Xyl), 7.16 (d, 4H,  ${}^{3}J_{HH} =$ 7.6 Hz, m-Xyl), 7.12 (dd,  ${}^{3}J_{HH} = 7.6$  Hz,  ${}^{4}J_{HP} = 3.5$  Hz, m-C<sub>6</sub>H<sub>3</sub>), 2.12 (s, 12H, CH<sub>3</sub>), 1.19 (d,  ${}^{2}J_{HP} = 10.4 \text{ Hz}$ , P-CH<sub>3</sub>).  ${}^{13}C\{{}^{1}H\}$  NMR (125) MHz, CDCl<sub>3</sub>, 25 °C,  $\delta$ ): 145.2 (d,  ${}^2J_{CP} = 10$  Hz, o- $C_6H_3$ ), 139.4 (d,  ${}^{3}J_{CP} = 5 \text{ Hz}$ , ipso-Xyl), 135.1 (o-Xyl), 130.9 (d,  ${}^{4}J_{CP} = 3 \text{ Hz}$ , p-C<sub>6</sub>H<sub>3</sub>), 130.1 (d,  ${}^{3}J_{CP} = 8 \text{ Hz}, m-C_{6}H_{3}$ ), 127.6 (p-Xyl), 127.1 (m-Xyl), 125.6 (d,  ${}^{1}J_{CP} = 57$  Hz, ipso-C<sub>6</sub>H<sub>3</sub>), 20.8 (CH<sub>3</sub>), 16.3 (d,  ${}^{1}J_{CP} = 39$ , P-CH<sub>3</sub>).  ${}^{31}P\{{}^{1}H\}$  NMR (161.9 MHz, CDCl<sub>3</sub>, 25 °C,  $\delta$ ): -3.7.

ES-MS(+) m/z: 601.11 ([M + Na<sup>+</sup>]<sup>+</sup>, Calcd 601.11), 543.15 ([M - Cl<sup>-</sup>]<sup>+</sup>, Calcd 543.15), 889.33 ([AuP<sub>2</sub>]<sup>+</sup>, Calcd 890.34), 617.08 ([M + K<sup>+</sup>]<sup>+</sup>, Calcd 617.08), 585.14 ([M + Li<sup>+</sup>]<sup>+</sup>, Calcd 585.14).

Synthesis of [AuCl(PCyp<sub>2</sub>Ar<sup>Xyl2</sup>)], AuCl**P2**. The synthesis of AuClP2 was performed following the same procedure as for AuClP1 by substitution of P1 for P2 (336.2 mg, 0.74 mmol). Yield 80% (576.5 mg). <sup>1</sup>H NMR (400 MHz, CDCl<sub>3</sub>, 25 °C, δ): 7.38 (td, 1H,  ${}^{3}J_{HH} = 7.6$  Hz,  ${}^{5}J_{HP} = 1.0$  Hz,  $p\text{-}C_{6}H_{3}$ ), 7.16 (dd, 2H,  $J_{HH} = 8.0$ , 7.1 Hz, p-Xyl), 7.07–7.06 (m, 4H, m-Xyl), 7.01 (dd, 2H,  ${}^{3}J_{HH} = 7.6$ Hz,  ${}^{4}J_{HP} = 1.7$  Hz, m-C<sub>6</sub> $H_3$ ), 2.06 (s, 12H, C $H_3$ ), 1.87–0.94 (m, 18H, Cyp).  ${}^{13}C\{{}^{1}H\}$  NMR (125 MHz, CDCl<sub>3</sub>, 25 °C,  $\delta$ ): 147.0 (d,  ${}^{2}J_{CP} = 9$ Hz, o- $C_6H_3$ ), 140.3 (d,  ${}^3J_{CP}$  = 5 Hz, ipso-Xyl), 135.3 (o-Xyl), 131.2 (d,  $^{3}J_{CP} = 7 \text{ Hz}, m-C_{6}H_{3}), 130.1 \text{ (d, } ^{4}J_{CP} = 2 \text{ Hz}, p-C_{6}H_{3}), 127.7 \text{ (d, } ^{1}J_{CP} = 2 \text{ Hz}, p-C_{6}$ 47 Hz,  $ipso-C_6H_3$ ), 127.3 (p-Xyl), 126.8 (m-Xyl), 37.1 (d,  ${}^1J_{CP} = 35$ Hz, P-CH), 34.1 (d,  $J_{CP} = 8$  Hz,  $CH_2$ ), 31.4 (d,  $J_{CP} = 7$  Hz,  $CH_2$ ), 24.1 (d,  $J_{CP} = 12$  Hz,  $CH_2$ ), 23.8 (d,  $J_{CP} = 14$  Hz,  $CH_2$ ), 20.5 ( $CH_3$ ). <sup>31</sup>P{<sup>1</sup>H} NMR (161.9 MHz, CDCl<sub>3</sub>, 25 °C,  $\delta$ ): 51.5. ES-MS(+) m/z: 709.20 ([M + Na<sup>+</sup>]<sup>+</sup>, Calcd 709.20), 651.24 ([M - Cl<sup>-</sup>]<sup>+</sup>, Calcd 651.25), 692.27 ( $[M - Cl + ACN]^+$ , Calcd 692.27).

Synthesis of [Au(carbazolyl)(PMe<sub>2</sub>Ar<sup>Xyl2</sup>)], 1a. Carbazole (25.1 mg, 0.15 mmol) and AuClP1 (89.2 mg, 0.15 mmol) were added to a previously prepared solution of NaO<sup>t</sup>Bu (14.4 mg, 0.15 mmol) in dry THF (10 mL). The suspension was maintained under stirring at room temperature overnight. Then, the solution is filtered through Celite and evaporated until dryness. After that, the solid obtained was recrystallized with dichloromethane/hexane to obtain the pure product. Yield 52% (56.9 mg). <sup>1</sup>H NMR (400 MHz, CDCl<sub>3</sub>, 25 °C, δ): 8.11–8.08 (m, 2H, CH<sub>Ar</sub>), 7.66 (td, 1H,  ${}^{3}J_{HH}$  = 7.5 Hz,  ${}^{5}J_{HP}$  = 2 Hz, p-C<sub>6</sub> $H_3$ ), 7.46–7.44 (m, 2H,  $CH_{Ar}$ ), 7.32–7.28, (m, 2H, p-Xyl), 7.17–7.03 (m, 10H,  $CH_{Arr}$  *m*-Xyl, m-C<sub>6</sub>H<sub>3</sub>), 2.22 (s,12H,  $CH_3$ ), 1.27 (d,  ${}^2J_{HP}$  = Hz, P– $CH_3$ ).  ${}^{13}C\{{}^{1}H\}$  NMR (75 MHz, CDCl<sub>3</sub>, 25 °C,  $\delta$ ): 149.3 (C<sub>Ar</sub>), 146.1 (d,  ${}^{2}J_{CP} = 10 \text{ Hz}$ ,  $o - C_{6}H_{3}$ ), 140.5 (d,  ${}^{3}J_{CP} = 5 \text{ Hz}$ , ipso-Xyl), 136.3 (o-Xyl), 131.4 (p- $C_6H_3$ ), 131.1 (d,  $^3J_{CP}=8$  Hz, m- $C_6H_3$ ), 128.7 (p-Xyl), 128.1 (m-Xyl), 127.1 (d,  ${}^{1}J_{CP} = 55$  Hz, ipso- $C_6H_3$ ), 124.1 (d,  ${}^3J_{CP} = 3$  Hz,  $C_{Ar}$ ), 123.6, 119.6, 119.2, 116.1, 113.7  $(C_{Ar})$ , 21.9  $(CH_3)$ , 16.9  $(d, {}^{1}J_{CP} = 39, P - CH_3)$ .  ${}^{31}P\{{}^{1}H\}$  NMR (161.9) MHz, CDCl<sub>3</sub>, 25 °C,  $\delta$ ): -0.9. ES-MS(+) m/z: 710.2236 ([M + H<sup>+</sup>]<sup>+</sup>,

Calcd 710.2200), 732.2052 ([M + Na<sup>+</sup>]<sup>+</sup>, Calcd 732.2100). Synthesis of [Au(carbazolyl)(PCyp<sub>2</sub>Ar<sup>Xyl2</sup>)], **2a**. The synthesis of **2a** was performed following the same procedure as for **1a** by substitution of AuClP1 for AuClP2 (145.9 mg, 0.2 mmol). Yield 46% (79.9 mg). <sup>1</sup>H NMR (400 MHz, CDCl<sub>3</sub>, 25 °C,  $\delta$ ): 8.08 (dd, 2H,  $J_{\rm HH}$  = 7.7, 0.7 Hz,  $CH_{\rm Ar}$ ), 7.57 (td, 1H,  $^3J_{\rm HH}$  = 7.6 Hz,  $^5J_{\rm HP}$  = 1.7 Hz, p-C<sub>6</sub>H<sub>3</sub>), 7.30–7.25 (m, 4H,  $CH_{\rm Ar}$ ), 7.16 (dd, 2H,  $CH_{\rm Ar}$ ), 7.02 (m, 2H,  $CH_{\rm Ar}$ ), 6.87–6.85 (m, 4H,  $CH_{\rm Ar}$ ), 6.58 (br, 2H,  $CH_{\rm Ar}$ ), 6.57–6.85 (m, 4H,  $CH_{\rm Ar}$ ), 6.58 (br, 2H,  $CH_{\rm Ar}$ ), 6.87–6.85 (m, 4H,  $CH_{\rm Ar}$ ), 6.58 (br, 2H,  $CH_{\rm Ar}$ ), 6.87–6.85 (m, 4H,  $CH_{\rm Ar}$ ), 6.58 (br, 2H,  $CH_{\rm Ar}$ ), 6.87–6.85 (m, 4H,  $CH_{\rm Ar}$ ), 6.58 (br, 2H,  $CH_{\rm Ar}$ ), 6.58 (br, 2H,  $CH_{\rm Ar}$ ), 6.87–6.85 (m, 4H,  $CH_{\rm Ar}$ ), 6.58 (br, 2H,  $CH_{\rm Ar}$ ), 6.87–6.85 (m, 4H,  $CH_{\rm Ar}$ ), 6.58 (br, 2H,  $CH_{\rm AR}$ )

 $C_6H_3$ ), 2.34–2.25 (m, 2H, Cyp), 2.14 (s, 12H, CH<sub>3</sub>), 1.95–1.84 (m, 6H, Cyp), 1.76–1.40 (m, 10H, Cyp).  $^{13}C\{^1H\}$  NMR (75 MHz, CDCl<sub>3</sub>, 25 °C,  $\delta$ ): 149.5 (C<sub>Ar</sub>), 148.3 (d,  $^2J_{CP}$  = 10 Hz, o- $C_6H_3$ ), 140.3 (d,  $^3J_{CP}$  = 5 Hz, ipso-Xyl), 135.9 (o-Xyl), 132.2 (d,  $^3J_{CP}$  = 7 Hz, m- $C_6H_3$ ), 131.2 (p- $C_6H_3$ ), 128.5 (d,  $^1J_{CP}$  = 52 Hz, ipso- $C_6H_3$ ), 128.2 (p-Xyl), 127.8 (m-Xyl), 124 (C<sub>Ar</sub>), 123.2, 119.4, 115.4, 113.9 (C<sub>Ar</sub>), 38.0 (d,  $^1J_{CP}$  = 41 Hz, p-CH), 35.3 (d,  $J_{CP}$  = 8 Hz, CH<sub>2</sub>), 32.4 (d,  $J_{CP}$  = 7 Hz, CH<sub>2</sub>), 25.6 (d,  $J_{CP}$  = 11 Hz, CH<sub>2</sub>), 25.4 (d,  $J_{CP}$  = 13 Hz, CH<sub>2</sub>), 21.6 (CH<sub>3</sub>).  $^{31}P\{^1H\}$  NMR (161.9 MHz, CDCl<sub>3</sub>, 25 °C,  $\delta$ ): 49.4. ES-MS(+)m/z: 820.3272 ([M + H<sup>+</sup>]<sup>+</sup>, Calcd 820.3200), 843.3477 ([M + Na<sup>+</sup>]<sup>+</sup>, Calcd 841.3000).

Synthesis of [Au(phenanthrenyl)(PMe2ArXyl2)], 1b. 9-Phenanthreneboronic acid (55.3 mg, 0.25 mmol) and AuClP1 (144 mg, 0.25 mmol) were added to a previously prepared solution of Cs2CO3 (122.2 mg, 0.38 mmol) in dry 2-propanol (10 mL). The suspension was stirred overnight at room temperature. Then, the solution was filtered with Celite and evaporated until dryness. The solid obtained was then recrystallized with dichloromethane/hexane to obtain the product in a pure form. Yield 57% (102.2 mg). <sup>1</sup>H NMR (400 MHz, CDCl<sub>3</sub>, 25 °C,  $\delta$ ): 8.68–8.65 (m, 1H, CH<sub>Ar</sub>), 8.62–8.60 (m, 1H,  $CH_{Ar}$ ), 8.32 (dd, 1H,  $J_{HH}$  = 7.5, 2 Hz,  $CH_{Ar}$ ), 7.78 (dd, 1H, J = 6.6, 2.0 Hz,  $CH_{Ar}$ ), 7.71–7.70 (m, 1H,  $p-C_6H_3$ ), 7.57–7.46 (m, 5H, CH<sub>Ar</sub>), 7.23–7.21 (m, 2H, p-Xyl), 7.16–7.14 (m, 4H, m-Xyl), 7.13 (dd,  ${}^{3}J_{HH} = 7.6 \text{ Hz}$ ,  ${}^{4}J_{HP} = 3.0 \text{ Hz}$ ,  $m\text{-}C_{6}H_{3}$ ), 2.22 (s, 12H, CH<sub>3</sub>), 1.14 (d, 6H, J = 8.1 Hz, P-CH<sub>3</sub>). <sup>13</sup>C{<sup>1</sup>H} NMR (75 MHz, CDCl<sub>3</sub>, 25 °C, δ): 173.0 ( $C_{Ar}$ ), 171.4 ( $C_{Ar}$ ), 146.0 ( $d_{r}$   $^{2}J_{CP}$  = 10 Hz, o- $C_{6}H_{3}$ ), 141.6  $(C_{Ar})$ , 141.1 (d,  ${}^{3}J_{CP} = 5$  Hz,  $ipso-C_{6}H_{3}$ ), 136.6  $(C_{Ar})$ , 136.5 (o-Xyl), 135.0 ( $C_{Ar}$ ), 132,6 (d,  $J_{CP}$  = 7 Hz,  $C_{Ar}$ ), 131.0 (p- $C_6$ H<sub>3</sub>), 130,8 (d,  $J_{CP}$ = 8 Hz, m- $C_6$ H<sub>3</sub>), 130.4 (d,  $J_{CP}$  = 6 Hz,  $C_{Ar}$ ), 130.2, 129.2 ( $C_{Ar}$ ), 128.3 (p-Xyl), 128.0 (m-Xyl), 127.8 ( $C_{Ar}$ ), 125.4 (d,  $^{1}J_{CP}$  = 58 Hz, ipso- $C_{3}H_{6}$ ), 124.8, 124.6, 122.4, 22.3 ( $C_{Ar}$ ), 22.0 (CH<sub>3</sub>), 16.5 (d,  $^{1}J_{CP}$  = 32 Hz, P-CH<sub>3</sub>).  ${}^{31}$ P{ ${}^{1}$ H} NMR (161.9 MHz, CDCl<sub>3</sub>, 25 °C,  $\delta$ ): 17.8. ES-MS(+) m/z: 721.2299 ([M + H<sup>+</sup>]<sup>+</sup>, Calcd 721.2220).

Synthesis of [Au(phenanthrenyl)(PCyp<sub>2</sub>Ar<sup>Xyl2</sup>)], **2b**. The synthesis of 2b was performed following the same procedure as for 1b by substitution of AuClP1 for AuClP2 (101.9 mg, 0.14 mmol). Yield 43% (52.9 mg). <sup>1</sup>H NMR (400 MHz, CDCl<sub>3</sub>, 25 °C, δ): 8.70 (d, 1H,  $J_{\rm HH}$  = 7.9 Hz,  $CH_{\rm Ar}$ ), 8.63 (d, 1H,  $J_{\rm HH}$  = 8.4 Hz,  $CH_{\rm Ar}$ ), 8.59 (d, 1H,  $J_{HH} = 8.0 \text{ Hz}, CH_{Ar}), 8.21 \text{ (dd, 1H, } J_{HH} = 7.8, 1.3 \text{ Hz}, CH_{Ar}), 7.91-$ 7.89 (m, 1H,  $CH_{Ar}$ ), 7.70–7.40 (m, 5H,  $CH_{Ar}$ , p- $C_6H_3$ , p-Xyl), 7.10 (dd, 2H, J = 1.6, 2.6 Hz,  $CH_{Ar}$ ), 7.00–6.93 (m, 6H, m- $C_6H_3$ , m-Xyl), 2.44-2.34 (m, 2H, Cyp), 2.14 (s, 12H, CH<sub>3</sub>), 2.0-1.40 (m, 16H, Cyp).  ${}^{13}C\{{}^{1}H\}$  NMR (75 MHz, CDCl<sub>3</sub>, 25 °C,  $\delta$ ): 177.2 (C<sub>Ar</sub>), 175.7  $(C_{Ar})$ , 148.7 (d,  ${}^{2}J_{CP} = 10 \text{ Hz}$ ,  $o - C_{6}H_{3}$ ), 142.0 (ipso-Xyl), 141. Eight  $(C_{Ar})$ , 136.2 (o-Xyl), 135.6, 134.8, 132.6  $(C_{Ar})$ , 132.5  $(d, {}^{1}J_{CP} = 38)$ Hz,  $ipso-C_6H_3$ ), 132.0 (d,  ${}^3J_{CP} = 7$  Hz,  $m-C_6H_3$ ), 130.6 ( $p-C_6H_3$ ), 130.4 (C<sub>Ar</sub>), 128.9 (C<sub>Ar</sub>), 127.9 (p-Xyl), 127.8 (m-Xyl), 127.4, 125.6, 124.5, 124.2, 124.1, 122.2 ( $C_{Ar}$ ), 38.1 (d,  $^{1}J_{CP}$  = 28 Hz, P-CH), 34.7 (d,  $J_{\rm CP}$  = 10 Hz, CH<sub>2</sub>), 32.0 (d,  $J_{\rm CP}$  = 8 Hz, CH<sub>2</sub>), 25.7 (d,  $J_{\rm CP}$  = 11 Hz, CH<sub>2</sub>), 25.4 (d,  $J_{\rm CP}$  = 13 Hz, CH<sub>2</sub>), 21.7 (CH<sub>3</sub>). <sup>31</sup>P{<sup>1</sup>H} NMR (161.9 MHz, CDCl<sub>3</sub>,  $\delta$ ): 57.5. ES-MS(+) m/z: 829.3247 ([M + H<sup>+</sup>]<sup>+</sup>, Calcd 829.3159).

Synthesis of [Au(dibenzofuranyl)(PMe<sub>2</sub>Ar<sup>Xyl2</sup>)], 1c. The synthesis of 1c was performed following the same procedure as for 1b by substitution of 9-phenanthreneboronic acid for dibenzo-4-boronic acid (8.5 mg, 0.04 mmol). Yield 59% (16.8 mg). <sup>1</sup>H NMR (400 MHz, CDCl<sub>3</sub>, 25 °C, δ): 8.06–8.02 (m, 1H, CH<sub>Ar</sub>), 7.98 (dd, 1H,  $J_{\rm HH}$  = 7.6, 1.3 Hz, CH<sub>Ar</sub>), 7.91–7.89 (m, 1H, p-C<sub>6</sub>H<sub>3</sub>), 7.70–7.68 (m, 1H, CH<sub>Ar</sub>), 7.57–7.23 (m, 6H, CH<sub>Ar</sub>), 7.24–7.17 (m, 2H, CH<sub>Ar</sub>), 7.15–7.11 (m, 6H, m-C<sub>6</sub>H<sub>3</sub>, p-Xyl), 2.25 (s, 12H, CH<sub>3</sub>), 1.14 (d, 6H,  ${}^2J_{\rm HP}$  = 8.4 Hz, p-CH<sub>3</sub>). <sup>13</sup>C{ $^1$ H} NMR (75 MHz, CDCl<sub>3</sub>, 25 °C, δ): 163.9, 155.8, 152.0, 150.4 ( $C_{\rm Ar}$ ), 146.1 (d,  ${}^2J_{\rm CP}$  = 10 Hz, o-C<sub>6</sub>H<sub>3</sub>), 141.1 (d,  ${}^3J_{\rm CP}$  = 4 Hz, ipso-Xyl), 137.8 ( $C_{\rm Ar}$ ), 136.5 (o-Xyl), 130.9 (p-C<sub>6</sub>H<sub>3</sub>), 130.8 (d,  ${}^3J_{\rm CP}$  = 7 Hz, m-C<sub>6</sub>H<sub>3</sub>), 130.1 (d,  ${}^1J_{\rm CP}$  = 41 Hz, ipso-C<sub>6</sub>H<sub>3</sub>), 128.2 (p-Xyl), 127.9 (m-Xyl), 126.0, 125.7 ( $C_{\rm Ar}$ ), 122.2 (d,  $J_{\rm CP}$  = 5 Hz,  $C_{\rm Ar}$ ), 121.5, 120.4, 117.1, 111.3 ( $C_{\rm Ar}$ ), 22.0 (CH<sub>3</sub>), 16.5 (d,  ${}^1J_{\rm CP}$  = 32 Hz, p-CH<sub>3</sub>). <sup>31</sup>P{<sup>1</sup>H} NMR (161.9 MHz, CDCl<sub>3</sub>, 25 °C, δ): 16.4. ES-MS(+) m/z: 711.2077 ([M + H<sup>+</sup>]<sup>+</sup>, Calcd 711.2013).

Synthesis of [Au(dibenzofuranyl)(PCyp<sub>2</sub>Ar<sup>xy/2</sup>)], 2c. The synthesis of 2c was performed following the same procedure as for 1c by

substitution of AuClP1 for AuClP2 (165.5 mg, 0.23 mmol). Yield 41% (82.5 mg). <sup>1</sup>H NMR (400 MHz, CDCl<sub>3</sub>, 25 °C, δ): 7.88–7.85 (m, 1H,  $CH_{Ar}$ ), 7.63–7.60 (m, 1H,  $CH_{Ar}$ ), 7.52 (td, 1H,  $^3J_{HH}$  = 7.6 Hz,  ${}^{5}J_{HP} = 1.7$  Hz,  $p - C_{6}H_{3}$ ), 7.37 - 7.29 (m, 2H,  $CH_{Ar}$ ), 7.19 - 7.18(dd, 1H,  $J_{HH}$  = 7.6, 1.2 Hz,  $CH_{Ar}$ ), 7.21–7.17 (m, 2H, p-Xyl), 7.11 (dd, 2H, J = 7.6, 2.7 Hz,  $CH_{Ar}$ ), 7.05 (s, 6H, m-Xyl, m- $C_6H_3$ ), 2.39– 2.29 (m, 2H, Cyp), 2.13 (s, 12H, CH<sub>3</sub>), 2.01–1.70 (m, 10H, Cyp), 1.61–1.40 (m, 6H, Cyp).  $^{13}C\{^{1}H\}$  NMR (75 MHz, CDCl<sub>3</sub>, 25 °C, δ): 164.6, 156.0, 155.7, 154.6 ( $C_{Ar}$ ), 148.7 (d,  ${}^2J_{CP} = 10 \text{ Hz}$ ,  $o - C_6H_3$ ), 141.9 (d,  ${}^{3}J_{CP} = 5$  Hz, ipso-Xyl), 136.9 ( $C_{Ar}$ ), 136.4 (o-Xyl), 132.0, 131.9 (d,  ${}^{3}J_{CP} = 6 \text{ Hz}, m\text{-}C_{6}H_{3}), 130.6 (p\text{-}C_{6}H_{3}), 127.8 (p\text{-}Xyl), 127.7$ (m-Xyl), 127.1 (d,  ${}^{1}J_{CP} = 40 \text{ Hz}$ , ipso- $C_{6}H_{3}$ ), 126.1, 125.3 ( $C_{Ar}$ ), 121.8 (d,  $J_{CP} = 5$  Hz,  $C_{Ar}$ ), 121.2, 120.5, 116.3, 110.9 ( $C_{Ar}$ ), 38.1 (d,  $^{1}J_{CP} =$ 28 Hz, P-CH), 34.7 (d,  $J_{CP} = 10$  Hz,  $CH_2$ ), 32.0 (d,  $J_{CP} = 8$  Hz,  $CH_2$ ), 25.7 (d,  $J_{CP} = 11$  Hz,  $CH_2$ ), 25.3 (d,  $J_{CP} = 13$  Hz,  $CH_2$ ), 21.6 (CH<sub>3</sub>).  ${}^{31}P\{{}^{1}H\}$  NMR (161.9 MHz, CDCl<sub>3</sub>, 25 °C,  $\delta$ ): 56.7. ES-MS(+) m/z: 819.3023 ([M + H<sup>+</sup>]<sup>+</sup>, Calcd 819.2952).

## ASSOCIATED CONTENT

# **Supporting Information**

The Supporting Information is available free of charge at https://pubs.acs.org/doi/10.1021/acs.inorgchem.4c04964.

Additional details on the characterization data including NMR, X-ray crystallography and photophysical data; computational data; catalysis screening and information on the obtained compounds (PDF)

#### **Accession Codes**

Deposition Numbers 2300097–2300100 contain the supplementary crystallographic data for this paper. These data can be obtained free of charge via the joint Cambridge Crystallographic Data Centre (CCDC) and Fachinformationszentrum Karlsruhe Access Structures service.

# AUTHOR INFORMATION

## **Corresponding Authors**

M. Carmen Nicasio – Departamento de Química Inorgánica, Universidad de Sevilla, 41012 Seville, Spain; o orcid.org/ 0000-0002-6485-2953; Email: mnicasio@us.es

João Carlos Lima — LAQV-REQUIMTE, Departamento de Química, Faculdade de Ciências e Tecnologia, Universidade Nova de Lisboa, 2829-516 Caparica, Portugal; ⊚ orcid.org/0000-0003-0528-1967; Email: lima@fct.unl.pt

Laura Rodríguez — Departament de Química Înorgànica i Orgànica, Secció de Química Inorgànica, Universitat de Barcelona, and Institut de Nanociència i Nanotecnologia (IN2UB), 08028 Barcelona, Spain; orcid.org/0000-0003-1289-1587; Email: laurarodriguezr@ub.edu

# **Authors**

Araceli de Aquino – Departament de Química Inorgànica i Orgànica, Secció de Química Inorgànica, Universitat de Barcelona, and Institut de Nanociència i Nanotecnologia (IN2UB), 08028 Barcelona, Spain

Nazaret Santamaría — Departamento de Química Inorgánica, Universidad de Sevilla, 41012 Seville, Spain

Artur J. Moro – LAQV-REQUIMTE, Departamento de Química, Faculdade de Ciências e Tecnologia, Universidade Nova de Lisboa, 2829-516 Caparica, Portugal

David Aguilà – Departament de Química Inorgànica i Orgànica, Secció de Química Inorgànica, Universitat de Barcelona, and Institut de Nanociència i Nanotecnologia (IN2UB), 08028 Barcelona, Spain

Auxiliadora Prieto – Departamento de Química Inorgánica, Universidad de Sevilla, 41012 Seville, Spain

Complete contact information is available at: https://pubs.acs.org/10.1021/acs.inorgchem.4c04964

#### Notes

The authors declare no competing financial interest.

# ACKNOWLEDGMENTS

The authors are grateful to the Ministerio de Ciencia e Innovación of Spain (project numbers PID2022-139296NB-I00, PID2020-113797RB-C22, and CNS2022-135816) and the Spanish network, Organometallic Chemistry for Sustainable Solutions — OASIS (RED2022-134074-T). This article is also based upon work from COST Action CA22131, LUCES Supramolecular LUminescent Chemosensors for Environmental Security, supported by COST (European Cooperation in Science and Technology). This research used resources of the ALBA synchrotron. The corresponding crystallographic measurements were performed with the collaboration of ALBA staff at BL13-XALOC beamline.

## REFERENCES

- (1) Zhou, X.; Liang, H.; Jiang, P.; Zhang, K. Y.; Liu, S.; Yang, T.; Zhao, Q.; Yang, L.; Lv, W.; Yu, Q.; Huang, W. Multifunctional Phosphorescent Conjugated Polymer Dots for Hypoxia Imaging and Photodynamic Therapy of Cancer Cells. *Adv. Sci.* **2016**, *3*, 1500155.
- (2) Zhou, Y.; Qin, W.; Du, C.; Gao, H.; Zhu, F.; Liang, G. Long-Lived Room-Temperature Phosphorescence for Visual and Quantitative Detection of Oxygen. *Angew. Chem., Int. Ed.* **2019**, *131*, 12230.
- (3) Brandt, J. R.; Wang, X.; Yang, Y.; Campbell, A. J.; Fuchter, M. J. Circularly Polarized Phosphorescent Electroluminescence with a High Dissymmetry Factor from PHOLEDs Based on a Platinahelicene. *J. Am. Chem. Soc.* **2016**, *138*, 9743.
- (4) Song, W.; Gao, L.; Zhang, T.; Huang, J.; Su, J. [1,2,4]Triazolo-[1,5-a]pyridine-Based Host Materials for High-Performance Red PHOLEDs with External Quantum Efficiencies over 23%. *J. Lumin.* **2019**, 206, 386.
- (5) Han, J.; Duan, P.; Li, X.; Liu, M. Amplification of Circularly Polarized Luminescence through Triplet—Triplet Annihilation-Based Photon Upconversion. J. Am. Chem. Soc. 2017, 139, 9783.
- (6) Song, E.; Han, X.; Zhou, Y.; Wei, Y.; Jiang, X. F.; Ye, S.; Zhou, B.; Xia, Z.; Zhang, Q. Long-Lived Photon Upconversion Phosphorescence in RbCaF<sub>3</sub><sup>2+</sup>, Yb<sup>3+</sup> and the Dynamic Color Separation Effect. *iScience* **2019**, *19*, 597.
- (7) Eng, J.; Hagon, J.; Penfold, T. J. D-A<sub>3</sub> TADF Emitters: The Role of the Density of States for Achieving Faster Triplet Harvesting Rates. *J. Mater. Chem. C* **2019**, *7*, 12942.
- (8) Mihaly, J. J.; Phillips, A. T.; Malloy, J. T.; Marsh, Z. M.; Zeller, M.; Haley, J. E.; De La Harpe, K.; Grusenmeyer, T. A.; Gray, T. G. Synthesis and Photophysical Properties of Laterally Asymmetric Digold(I) Alkynyls and Triazolyl: Ancillary Ligand and Organic Functionality Dictate Excited-State Dynamics. *Organometallics* **2020**, 39, 489.
- (9) Mihaly, J. J.; Wolf, S. M.; Phillips, A. T.; Mam, S.; Yung, Z.; Haley, J. E.; Zeller, M.; De La Harpe, K.; Holt, E.; Grusenmeyer, T. A.; Collins, S.; Gray, T. G. Synthetically Tunable White-, Green-, and Yellow-Green-Light Emission in Dual-Luminescent Gold(I) Complexes Bearing a Diphenylamino-2,7-Fluorenyl Moiety. *Inorg. Chem.* 2022, 61, 1228.
- (10) Shen, Y.; Belbruno, J. J. Density Functional Theory Study of the Jahn—Teller Effect and Spin—Orbit Coupling for Copper and Gold Trimers. J. Phys. Chem. A 2005, 109, 512.
- (11) Marian, C. M. Spin-Orbit Coupling and Intersystem Crossing in Molecules. *Wiley Interdiscip. Rev.: Comput. Mol. Sci.* **2012**, 2 (2), 187–203.
- (12) Aliprandi, A.; Genovese, D.; Mauro, M.; De Cola, L. Recent Advances in Phosphorescent Pt(II) Complexes Featuring Metal-

- lophilic Interactions: Properties and Applications. Chem. Lett. 2015, 44 (8), 1152-1161.
- (13) Zheng, Q.; Borsley, S.; Nichol, G. S.; Duarte, F.; Cockroft, S. L. The Energetic Significance of Metallophilic Interactions. *Angew. Chem., Int. Ed.* **2019**, *58* (36), 12617–12623.
- (14) Otero De La Roza, A.; Mallory, J. D.; Johnson, E. R. Metallophilic Interactions from Dispersion-Corrected Density-Functional Theory. *J. Chem. Phys.* **2014**, *140* (18), 18A504.
- (15) Wang, Y. J.; Shi, X. Y.; Xing, P.; Zang, S. Q. Metallophilic Interactions Drive Supramolecular Chirality Evolution and Amplify Circularly Polarized Luminescence. *JACS Au* **2023**, 3 (3), 565–578.
- (16) Gil-Moles, M.; Gimeno, M. C.; López-De-Luzuriaga, J. M.; Monge, M.; Olmos, M. E.; Pascual, D. Tailor-Made Luminescent Polymers through Unusual Metallophilic Interaction Arrays Au···Au··· Ag···Ag. *Inorg. Chem.* **2017**, *56* (16), 9281–9290.
- (17) De Aquino, A.; Ward, J. S.; Rissanen, K.; Aullón, G.; Lima, J. C.; Rodríguez, L. Intra-vs Intermolecular Aurophilic Contacts in Dinuclear Gold(I) Compounds: Impact on the Population of the Triplet Excited State. *Inorg. Chem.* **2022**, *61* (4), 20931–20943.
- (18) Navarro, M.; Alférez, M. G.; De Sousa, M.; Miranda-Pizarro, J.; Campos, J. Dicoordinate Au(I)—Ethylene Complexes as Hydroamination Catalysts. *ACS Catal.* **2022**, *12* (5), 4227–4236.
- (19) Wang, W.; Hammond, G. B.; Xu, B. Ligand Effects and Ligand Design in Homogeneous Gold(I) Catalysis. *J. Am. Chem. Soc.* **2012**, 134 (13), 5697–5704.
- (20) (a) Lavallo, V.; Wright, J. H. I. I.; Tham, F. S.; Quinlivan, S. Perhalogenated Carba-Closo-Dodecaborate Anions as Ligand Substituents: Applications in Gold Catalysis. Angew. Chem., Int. Ed. 2013, 52 (13), 3172–3176. (b) Malhotra, D.; Mashuta, M. S.; Hammond, G. B.; Xu, B. A Highly Efficient and Broadly Applicable Cationic Gold Catalyst. Angew. Chem., Int. Ed. 2014, 53 (18), 4456–4460. (c) Handelmann, J.; Babu, C. N.; Steinert, H.; Schwarz, C.; Scherpf, T.; Kroll, A.; Gessner, V. Towards the Rational Design of Ylide-Substituted Phosphines for Gold(I)-Catalysis: From Inactive to Ppm-Level Catalysis. Chem. Sci. 2021, 12 (9), 4329–4340. (d) Ji, C.-L.; Han, J.; Li, T.; Zhao, C.-G.; Zhu, C.; Xie, J. Photoinduced Gold-Catalyzed Divergent Dechloroalkylation of gem-Dichloroalkanes. Nat. Catal. 2022, 5, 1098–1109.
- (21) Tang, Y.; Benaissa, I.; Huynh, M.; Vendier, L.; Lugan, N.; Bastin, S.; Belmont, P.; César, V.; Michelet, V. An Original L-Shape, Tunable N-Heterocyclic Carbene Platform for Efficient Gold(I) Catalysis. *Angew. Chem., Int. Ed.* **2019**, 58 (27), 7977–7982.
- (22) (a) Marín, M.; Moreno, J. J.; Navarro-Gilabert, C.; Alvarez, E.; Maya, C.; Peloso, R.; Nicasio, M. C.; Carmona, E. Synthesis, Structure, and Nickel Carbonyl Complexes of Dialkylterphenyl Phosphines. *Chem. Eur. J.* **2018**, 25 (1), 260–272. (b) Rama, R. J.; Maya, C.; Nicasio, M. C. Dialkylterphenyl Phosphine-Based Palladium Precatalysts for Efficient Aryl Amination of N-Nucleophiles. *Chem. Eur. J.* **2020**, 26 (5), 1064–1073. (c) Martín, M. T.; Marín, M.; Rama, R. J.; Álvarez, E.; Maya, C.; Molina, F.; Nicasio, M. C. Zero-Valent ML<sub>2</sub> Complexes of Group 10 Metals Supported by Terphenyl Phosphanes. *Chem. Commun.* **2021**, 57 (5), 3083–3089.
- (23) Kovács, G.; Lledós, A.; Ujaque, G. Hydroamination of Alkynes with Ammonia: Unforeseen Role of the Gold(I) Catalyst. *Angew. Chem., Int. Ed.* **2011**, *123* (45), 11343–11347.
- (24) (a) Huang, L.; Arndt, M.; Gooßen, K.; Heydt, H.; Gooßen, L. J. Late Transition Metal-Catalyzed Hydroamination and Hydroamidation. *Chem. Rev.* **2015**, *115* (6), 2596–2697. (b) Leung, C. H.; Baron, M.; Biffis, A. Gold-Catalyzed Intermolecular Alkyne Hydrofunctionalizations—Mechanistic Insights. *Catalysts* **2020**, *10* (10), 1210.
- (25) De Aquino, A.; Caparrós, F. J.; Truong, K.-N.; Rissanen, K.; Ferrer, M.; Jung, Y.; Choi, H.; Lima, J. C.; Rodríguez, L. Gold(I)-Doped Films: New Routes for Efficient Room Temperature Phosphorescent Materials. *Dalton Trans.* **2021**, *50* (11), 3806–3815. (26) Yun, S. J.; Seo, M. H.; Lee, S. Dibenzofuran Derivatives with Meta- and Para-Triphenylamine Substituents as Hole-Transporting Materials in Organic Light-Emitting Devices. *Dyes Pigm.* **2020**, *175*, 108121.

- (27) Jayaraman, J.; Ganapathy, A. S.; Thanikachalam, V.; Palanivel, J.; Sekar, P. Organic-Inorganic Hybrids Based on Phenanthrene-Functionalized Gold Nanoparticles for OLEDs. *J. Phys. Org. Chem.* **2017**, *31* (5), No. e3796.
- (28) Romanov, A. S.; Yang, L.; Jones, S. T. E.; Di, D.; Morley, O. J.; Drummond, B. H.; Reponen, A. P. M.; Linnolahti, M.; Credgington, D.; Bochmann, M. Dendritic Carbene Metal Carbazole Complexes as Photoemitters for Fully Solution-Processed OLEDs. *Chem. Mater.* **2019**, *31* (11), 3613–3625.
- (29) Osawa, M.; Hoshino, M.; Akita, M.; Wada, T. Synthesis and Characterization of Phenanthrylphosphine Gold Complex: Observation of Au-Induced Blue-Green Phosphorescence at Room Temperature. *Inorg. Chem.* **2005**, *44* (4), 1157–1163.
- (30) Osawa, M.; Hoshino, M.; Hashizume, D. Photophysics and Photochemistry of Biphenylyl Triphenylphosphine Gold(I) Complexes. *Chem. Phys. Lett.* **2007**, 436 (1), 89–94.
- (31) Falivene, L.; Cao, Z.; Petta, A.; Serra, L.; Poater, A.; Oliva, R.; Scarano, V.; Cavallo, L. Towards the Online Computer-Aided Design of Catalytic Pockets. *Nat. Chem.* **2019**, *11* (10), 872–879.
- (32) Marín, M.; Moreno, J. J.; Alcaide, M. M.; Álvarez, E.; López-Serrano, J.; Campos, J.; Nicasio, M. C.; Carmona, E. Evaluating Stereoelectronic Properties of Bulky Dialkylterphenyl Phosphine Ligands. J. Organomet. Chem. 2019, 896, 120–132.
- (33) Eusamio, J.; Medina, Y. M.; Córdoba, J. C.; Vidal-Ferran, A.; Sainz, D.; Gutiérrez, A.; Font-Bardia, M.; Grabulosa, A. Rhodium and Ruthenium Complexes of Methylene-Bridged, P-Stereogenic, Unsymmetrical Diphosphanes. *Dalton Trans.* **2023**, *52* (6), 2424–2432.
- (34) Huang, R.; Avó, J.; Northey, T.; Chaning-Pearce, E.; dos Santos, P. L.; Ward, J. S.; Data, P.; Etherington, M. K.; Fox, M. A.; Penfold, T. J.; Berberan-Santos, M. N.; Lima, J. C.; Bryce, M. R.; Dias, F. B. The Contributions of Molecular Vibrations and Higher Triplet Levels to the Intersystem Crossing Mechanism in Metal-Free Organic Emitters. J. Mater. Chem. C 2017, 5 (26), 6269–6280.
- (35) De Aquino, A.; Ward, J. S.; Rissanen, K.; Aullón, G.; Lima, J. C.; Rodríguez, L. Intra-vs Intermolecular Aurophilic Contacts in Dinuclear Gold(I) Compounds: Impact on the Population of the Triplet Excited State. *Inorg. Chem.* **2022**, *61* (4), 20931–20943.
- (36) Evans, R. C.; Douglas, P.; Burrows, H. D. Applied Photochemistry; Springer, 2014.
- (37) Wu, B.; Su, H.; Cheng, A.; Zhang, X.; Wang, T.; Zhang, G. The El-Sayed's Rule Analogy Enables Long-Lived Room Temperature Phosphorescence in Twisted Biphenyls. *Cell Rep. Phys. Sci.* **2023**, 4 (2), 101245.
- (38) Neither the Complexes 2(a-c) nor the Chloride Precursors AuClPx Were Catalytically Active in the Model Hydroamination Reaction (see Table S6 in the Supporting Information for Details).
- (39) (a) Lavallo, V.; Frey, G. D.; Donnadieu, B.; Soleilhavoup, M.; Bertrand, G. Homogeneous Catalytic Hydroamination of Alkynes and Allenes with Ammonia. *Angew. Chem., Int. Ed.* **2008**, *47* (28), 5224–5228. (b) Zeng, X.; Frey, G. D.; Kousar, S.; Bertrand, G. A Cationic Gold(I) Complex as a General Catalyst for the Intermolecular Hydroamination of Alkynes: Application to the One-Pot Synthesis of Allenes from Two Alkynes and a Sacrificial Amine. *Chem. Eur. J.* **2009**, *15* (13), 3056–3060. (c) Hesp, K. D.; Stradiotto, M. Stereoand Regioselective Gold-Catalyzed Hydroamination of Internal Alkynes with Dialkylamines. *J. Am. Chem. Soc.* **2010**, *132* (50), 18026–18034.
- (40) Ortega-Moreno, L.; Fernández-Espada, M.; Moreno, J. J.; Navarro-Gilabert, C.; Campos, J.; Conejero, S.; López-Serrano, J.; Maya, C.; Peloso, R.; Carmona, E. Synthesis, Properties, and Some Rhodium, Iridium, and Platinum Complexes of a Series of Bulky m-Terphenylphosphine Ligands. *Polyhedron* **2016**, *116*, 170–178.
- (41) Juanhuix, J.; Gil-Ortiz, F.; Cuní, G.; Colldelram, C.; Nicolás, J.; Lidón, J.; Boter, E.; Ruget, C.; Ferrer, S.; Benach, J. Developments in Optics and Performance at BL13-XALOC, the Macromolecular Crystallography Beamline at the ALBA Synchrotron. *J. Synchrotron Radiat.* 2014, 21 (4), 679–689.

- (42) Sheldrick, G. M. SHELXT—Integrated Space-Group and Crystal-Structure Determination. *Acta Crystallogr., Sect. A: Found. Crystallogr.* **2015**, 71 (1), 3–8.
- (43) Sheldrick, G. M. Crystal Structure Refinement with SHELXL. Acta Crystallogr., Sect. C: Struct. Chem. 2015, 71 (1), 3–8.
- (44) Frisch, M. J.; Trucks, G. W.; Schlegel, H. B.; Scuseria, G. E.; Robb, M. A.; Cheeseman, J. R.; Scalmani, G.; Barone, V.; Mennucci, B.; Petersson, G. A.; Nakatsuji, H.; Caricato, M.; Li, X.; Hratchian, H. P.; Izmaylov, A. F.; Bloino, J.; Zheng, G.; Sonnenberg, J. L.; Hada, M.; Ehara, M.; Toyota, K.; Fukuda, R.; Hasegawa, J.; Ishida, M.; Nakajima, T.; Honda, Y.; Kitao, O.; Nakai, H.; Vreven, T.; Montgomery, J. A.; Peralta, J. E.; Ogliaro, F.; Bearpark, M.; Heyd, J. J.; Brothers, E.; Kudin, K. N.; Staroverov, V. N.; Keith, T.; Kobayashi, R.; Normand, J.; Raghavachari, K.; Rendell, A.; Burant, J. C.; Iyengar, S. S.; Tomasi, J.; Cossi, M.; Rega, N.; Millam, J. M.; Klene, M.; Knox, J. E.; Cross, J. B.; Bakken, V.; Adamo, C.; Jaramillo, J.; Gomperts, R.; Stratmann, R. E.; Yazyev, O.; Austin, A. J.; Cammi, R.; Pomelli, C.; Ochterski, J. W.; Martin, R. L.; Morokuma, K.; Zakrzewski, V. G.; Voth, G. A.; Salvador, P.; Dannenberg, J. J.; Dapprich, S.; Daniels, A. D.; Farkas, O.; Foresman, J. B.; Ortiz, J. V.; Cioslowski, J.; Fox, D. J. Gaussian, 09.. Revision, B.1.; Gaussian, Inc.: Wallingford, CT, 2009.
- (45) Becke, A. Density-Functional Thermochemistry. III. The Role of Exact Exchange. *J. Chem. Phys.* **1993**, 98 (7), 5648–5652.
- (46) Lee, C.; Yang, W.; Parr, R. G. Development of the Colle-Salvetti Correlation-Energy Formula into a Functional of the Electron Density. *Phys. Rev. B* **1988**, *37* (2), 785–789.
- (47) Weigend, F.; Ahlrichs, R. Balanced Basis Sets of Split Valence, Triple Zeta Valence and Quadruple Zeta Valence Quality for H to Rn: Design and Assessment of Accuracy. *Phys. Chem. Chem. Phys.* **2005**, 7 (18), 3297–3305.
- (48) Schäfer, A.; Huber, C.; Ahlrichs, R. Fully Optimized Contracted Gaussian Basis Sets of Triple Zeta Valence Quality for Atoms Li to Kr. *J. Chem. Phys.* **1994**, *100* (8), 5829–5835.
- (49) Reed, A. E.; Curtiss, L. A.; Weinhold, F. Intermolecular Interactions from a Natural Bond Orbital, Donor-Acceptor Viewpoint. *Chem. Rev.* **1988**, *88* (6), 899–926.
- (50) Tomasi, J.; Mennucci, B.; Cammi, R. Quantum Mechanical Continuum Solvation Models. *Chem. Rev.* **2005**, *105* (8), 2999–3093.
- (51) Casida, M. E.; Jamorski, C.; Casida, K. C.; Salahub, D. R. Molecular Excitation Energies to High-Lying Bound States from Time-Dependent Density-Functional Response Theory: Characterization and Correction of the Time-Dependent Local Density Approximation Ionization Threshold. *J. Chem. Phys.* **1998**, *108* (11), 4439–4449.